11800–11809 *Nucleic Acids Research, 2021, Vol. 49, No. 20* *Published online 28 September 2021*
https://doi.org/10.1093/nar/gkab856

Oxidation alters the architecture of the phenylalanyl-tRNA synthetase editing domain to confer hyperaccuracy

Pooja Srinivas [1,2,3], Rebecca E. Steiner[4], Ian J. Pavelich[1,3,5], Ricardo Guerrero-Ferreira[6], Puneet Juneja[6], Michael Ibba[4] and Christine M. Dunham [1,3,*]

[1]Department of Biochemistry, Emory University School of Medicine, Atlanta, GA 30322, USA, [2]Molecular and Systems Pharmacology Graduate Program, Emory University, Atlanta, GA 30322, USA, [3]Antibiotic Resistance Center, Emory University, Atlanta, GA 30322, USA, [4]Department of Microbiology, The Ohio State University, Columbus, OH 43210, USA, [5]Department of Chemistry, Emory University, Atlanta, GA 30322, USA and [6]Robert P. Apkarian Integrated Electron Microscopy Core, Emory University School of Medicine, Atlanta, GA 30322, USA

Received July 29, 2021; Revised September 07, 2021; Editorial Decision September 08, 2021; Accepted September 16, 2021

ABSTRACT

High fidelity during protein synthesis is accomplished by aminoacyl-tRNA synthetases (aaRSs). These enzymes ligate an amino acid to a cognate tRNA and have proofreading and editing capabilities that ensure high fidelity. Phenylalanyl-tRNA synthetase (PheRS) preferentially ligates a phenylalanine to a $tRNA^{Phe}$ over the chemically similar tyrosine, which differs from phenylalanine by a single hydroxyl group. In bacteria that undergo exposure to oxidative stress such as *Salmonella enterica* serovar Typhimurium, tyrosine isomer levels increase due to phenylalanine oxidation. Several residues are oxidized in PheRS and contribute to hyperactive editing, including against mischarged Tyr-$tRNA^{Phe}$, despite these oxidized residues not being directly implicated in PheRS activity. Here, we solve a 3.6 Å cryo-electron microscopy structure of oxidized *S.* Typhimurium PheRS. We find that oxidation results in widespread structural rearrangements in the β-subunit editing domain and enlargement of its editing domain. Oxidization also enlarges the phenylalanyl-adenylate binding pocket but to a lesser extent. Together, these changes likely explain why oxidation leads to hyperaccurate editing and decreased misincorporation of tyrosine. Taken together, these results help increase our understanding of the survival of *S.* Typhimurium during human infection.

INTRODUCTION

Accurate protein synthesis is essential for cellular survival and one important family of enzymes involved in this process are the aminoacyl-tRNA synthetases (aaRS). These enzymes add an amino acid to cognate tRNAs at the 3′ terminal adenosine (A76) (1). The addition or charging of tRNAs is extremely accurate ($\sim 10^{-4}$) to ensure that correct amino acids are incorporated into proteins in a codon-specific manner (2). To enable this high fidelity, aaRSs discriminate between chemically-similar amino acids and have the ability to proofread and edit the incorrectly added amino acid (3). This proofreading capability allows for accurate translation to proceed.

aaRSs facilitate a two-step reaction to ligate an amino acid on a tRNA (4). First, the aaRS charges an amino acid with an adenylate group from ATP. Second, the aminoadenylate is ligated onto a tRNA. There are two structurally unrelated classes of aaRSs that differ in the location of the ligated aminoacyl group and in their editing functions (5,6). Class I synthetases aminoacylate the 2′-OH of the terminal A76 of a cognate tRNA (7,8), while Class II aaRSs generally aminoacylate tRNA at the 3′-OH of A76 (9). Class I aaRSs contain highly conserved editing domains and perform both pre-transfer editing, in which the misactivated amino acid-adenylate is hydrolyzed, and post-transfer editing, where the mischarged aminoacyl-tRNA is hydrolyzed (10–16). In contrast, class II aaRSs contain structurally diverse editing sites (17–19) and primarily rely on post-transfer editing. The diversity in class II aaRSs impart differences in their response to environmental stressors, such as increased thermal stability (20).

*To whom correspondence should be addressed. Tel: +1 404 712 1756; Fax: +1 404 727 2738. Email: christine.m.dunham@emory.edu
Present addresses:
Puneet Juneja, Cryo-EM Facility, University of Iowa, Ames, IA 50011-1079 USA; Michael Ibba, Schmid College of Science and Technology, Chapman University, Orange, CA 92866, USA.
Rebecca E. Steiner, College of Osteopathic Medicine, Lake Erie College of Osteopathic Medicine, Bradenton, FL 34211, USA.

Bacterial PheRS is a class II aaRS that functions as a heterotetramer, composed of two α subunits and two β subunits, $(\alpha\beta)_2$ (21). An amino acid, ATP, and tRNA bind in the aminoacylation domain of the α-subunits, and ligation occurs to the 2′-OH of $tRNA^{Phe}$, distinguishing PheRS from other class II aaRSs. The PheRS β-subunits contain the editing domain, where discrimination between Phe and Tyr occurs post-transfer via hydrolysis of misacylated $tRNA^{Phe}$ to prevent misincorporation of Tyr at Phe codons in the growing peptide chain. Tyr misincorporation rates are high (21), but low error rates can be reconciled by post-transfer editing (8,9,22). One aspect of proofreading is the requirement for Tyr-$tRNA^{Phe}$ to translocate ∼30 Å to the editing domain (22,23). Conserved residue His265 interacts with the aminoacyl group (22), and discrimination between Phe and Tyr occurs by βGlu334 recognition of the Tyr hydroxyl (24). Conserved βArg244 interacts with the $tRNA^{Phe}$ backbone at C75, while two catalytic waters are adjacent to the aminoacyl group that assist with residues βAsn254 and βThr354 to hydrolyze the ester bond between Tyr and the 2′-OH of $tRNA^{Phe}$ A76 (24). Residues βGly318 and βAla356 are also implicated in proofreading activity, as mutations in these residues prevent Tyr-$tRNA^{Phe}$ accommodation into the PheRS editing site (25).

PheRS proofreading activity is of particular importance when bacteria are subjected to oxidative stress (26,27). During oxidative stress, imbalances of reactive oxygen species damage various cellular components, including both proteins and nucleic acids (28–33). Damages include oxidation of free amino acids that alters endogenous amino acid pools whose limitation affects translational fidelity (29). Specifically, oxidative stress increases concentrations of *ortho, para,* and *meta*-Tyr isomers due to Phe oxidation, challenging PheRS proofreading by increasing the likelihood of $tRNA^{Phe}$ misacylation, and subsequent mistranslation (29).

Salmonella enterica serovar Typhimurium is a pathogen that infects the gastrointestinal (GI) tracts of humans and survives exposure to oxidative stress both in the GI tract and in the lysosomes of macrophages (27,34). Previous studies show that oxidized PheRS in *Salmonella enterica* serovar Typhimurium is hyperaccurate during oxidative conditions, increasing translational fidelity (25). Upon hydrogen peroxide (H_2O_2) treatment, PheRS displays increased proofreading activity and lower misacylation rates without changes in canonical aminoacylation activity, protecting cells from mistranslation under adverse growth conditions. Several residues located throughout PheRS become oxidized resulting in changes to secondary structural features (25). Here, we solved a 3.6 Å cryogenic-EM (cryo-EM) structure of the oxidized *S*. Typhimurium editing-deficient PheRS βG318W to assess structural changes that may contribute to increased proofreading. We report that PheRS oxidation induces conformational rearrangements of both the α and β subunits providing a rationale for hyperaccuracy during oxidative stress.

MATERIALS AND METHODS

PheRS expression and purification

Salmonella enterica serovar Typhimurium PheS and PheT βG318W proteins, encoding the α- and β-subunit, respectively, were purified as previously described (25). Briefly, PheRS was affinity purified (TALON), fractions containing protein were pooled, concentrated and dialyzed overnight in sample buffer (50 mM Tris pH 7.5, 100 mM KCl, 5 mM $MgCl_2$, 3 mM 2-mercaptoethanol, 5% glycerol). For storage at −80°C, PheRS was dialyzed 4 h in sample buffer containing 50% glycerol.

Cryo-EM sample preparation

Purified PheRS was dialyzed at 4°C for 4 h in a sample buffer containing 5 mM H_2O_2. Three μL of oxidized PheRS at 1.5 mg/ml was incubated for 10 s at 4°C on freshly glow-discharged grids (1.2/1.3 300 mesh Cu Quantifoil). Grids were blotted for 3 s at 100% humidity, plunged into liquid ethane with a Vitrobot Mark IV (FEI), and stored in liquid nitrogen.

Electron microscopy, image processing, and data analysis

A 1330 micrograph dataset was acquired using a Talos Arctica transmission electron microscope (ThermoFisher) operating at 200 keV with BioQuantum/K2 Summit direct electron detector (Gatan). Micrographs were collected at a pixel size of 1.04 Å/pixel at a defocus range of −0.5 to −3.5 μm. A total dose of 64.67 e/$Å^2$ per micrograph was fractioned into 48-frame movies with 12 s exposure time.

Image processing was conducted in Relion 3.0 (35). Motion correction and dose weighting was done using MotionCorr2 (36), and contrast transfer function parameters were estimated using Gctf (37). Laplacian of Gaussian algorithm was used to pick particles and generate templates for 2D-referenced based autopicking. Several rounds of 2D-reference based autopicking were conducted, with incorrectly selected particles discarded after reference-free 2D class averaging. An initial three-dimensional refinement with C2 symmetry was conducted using a previously published PheRS structure (PDB code 4P71 (38)) low-pass filtered to 45-Å in Chimera as a reference map (39) (Supplementary Figure S1). Three-dimensional refinement was followed by a 3D classification step, with poorly aligned particles discarded. A total of 204 902 particles were finally selected and subjected to particle polishing, 3D refinement, CTF refinement, and post-processing to yield a final reconstruction of 3.6 Å. Resolution estimations were calculated from Fourier shell correlations (FSC) at 0.143 between the two independently refined half-maps. Local resolution was calculated in Relion. The final map was refined and validated in PHENIX (40) and modeled with PDB code 3PCO (14). Coot (41) and UCSF ChimeraX (42) were used for model building.

Maps were analyzed using UCSF Chimera (39) and ChimeraX (42). Global structural alignments and RMSD calculations were conducted in ChimeraX, using the matchmaker tool which creates a global sequence alignment then fits aligned residue pairs (43). Distance calculations were all conducted in ChimeraX, from the Cα carbon of a residue. Figures were created using UCSF Chimera and ChimeraX.

RESULTS

Global structural impact of oxidation on PheRS βG318W

Treatment of *S*. Typhimurium wild-type (WT) and editing-deficient PheRS βG318W with H_2O_2 results in different residues becoming oxidized (25). The PheRS βG318W variant has a 7.5-fold reduction in proofreading due to the prevention of Tyr-tRNA^{Phe} binding in the editing site, likely by steric hindrance (24). Both *S*. Typhimurium oxidized WT and PheRS βG318W show increased proofreading capacity, with PheRS βG318W displaying the most pronounced effect with a >3-fold increase in Tyr-tRNA^{Phe} proofreading (25). Several PheRS βG318W residues were oxidized across both the α- and β-subunits but outside of catalytic regions, and thus it is unclear how increased proofreading results. To define the structural changes that PheRS undergoes during oxidative stress, we solved a 3.6-Å resolution structure of oxidized PheRS βG318W by single particle cryo- EM (Figure 1A; Supplementary Table S1, Supplementary Figure S1). PheRS adopts a heterotetrametric conformation composed of two α-subunits and two β-subunits $(\alpha\beta)_2$ with the α-subunit containing the aminoacylation catalytic domain (residues 108–307) and the β-subunit containing the editing domain (residues 216–354) (14,44–47) (Figure 1C and D). Due to the resolution, it is not possible to resolve the oxidation of specific residues (Figure 1B), but mass spectrometry revealed extensive oxidation under treatment conditions (25).

PheRS undergoes a conformational change upon tRNA^{Phe} binding (44,45), including the ordering of the N-terminal coiled-coil domain of the α-subunit (residues 1–88) (Figure 1C) (48). This region is not resolved in our structure likely because this structure is in the absence of tRNA^{Phe} (Figure 1A). *S*. Typhimurium PheRS is similar to the previously published *Pseudomonas aeruginosa* apo-PheRS structure (apo-*Pa*PheRS) (PDB code 4P71; root mean square deviation (RMSD) of ∼2.9 Å comparing the Cα of 790 residues) (38). *S*. Typhimurium PheRS and *Pa* PheRS share high sequence identity between both subunits (51.5% for the β-subunits and 65.7% for the α-subunits) and adopt identical tertiary folds (Supplementary Figures S2A and S3). For these reasons, and because our structure is also apo, all future comparisons will be made to apo-*Pa*PheRS unless otherwise noted.

Oxidation induces conformational changes in the PheRS βG318W catalytic domains

Different residues are oxidized in wild-type versus the PheRS βG318W editing-deficient variant, likely due to differences in the overall architecture (25). Six residues become oxidized in PheRS βG318W, which are located across the enzyme domains, with five residues in the β-editing domain and one residue in the α-aminoacylation domain (25) (Figure 1B; Supplementary Table S2). Comparison of PheRS βG318W with apo-*Pa*PheRS reveals that oxidized βMet280 and βLys282 undergo large changes in the position of their backbone (6.7 and 8.6 Å, respectively) while their side chain conformation is minimally impacted (Figure 2B and C). These residues are in the β-catalytic domain (Figure 2A) located adjacent to the editing site (Figure 1D). The entire β-strand surrounding the editing domain moves in towards the tRNA binding site in the β-subunit, likely contributing to the shift and conformational changes to editing site residues. Other residues within the β-subunit become oxidized yet this has little to no impact on their conformations. For example, ox-βLys184, ox-βTyr60 and ox-αAsn222 all have limited movement (Supplementary Figure S4), so it is unlikely that these rotamer changes play a significant role in the hyperaccuracy phenotype. In contrast, ox-βArg111 has a ∼180° rotation compared to *Ec*PheRS complexed with Phe-AMP (Supplementary Figure S4F), and a 16.6 Å movement inwards towards the editing domain compared to apo-*Pa*PheRS (Supplementary Figure S4E). However, since βArg111 is on the surface of the β-subunit, this difference may be a result from how apo-*Pa*PheRS packs in the crystal lattice (Supplementary Figure S5). Together, these data demonstrate that oxidation has a differential effect on local conformation of the PheRS residues, and oxidation of a given residue does not necessarily entail conformational change in that region.

PheRS oxidation causes structural rearrangements of its editing domain

After PheRS misacylates tRNA^{Phe} with a Tyr, Tyr-tRNA^{Phe} translocates to the editing domain in the β-subunit (Figure 3A) (22,24). In the editing domain, many residues surround Tyr to recognize and edit including βArg244, βAsn254, βHis265, βGlu334 and βThr354 (Figure 3B). The tRNA is typically stabilized by interactions of βArg244 with nucleotide C75, while βAsn254 and βThr354 are in proximity to the aminoacyl ester bond and involved in substrate binding and hydrogen bonding with catalytic waters (Figure 3B and C) (24). These residues were not demonstrated to be oxidized yet they display altered conformations (Figure 3D). βArg244, βAsn254 and βThr354 all shift away from the tRNA binding location at distances between ∼5.4 and 7.2Å (Figure 3D; Supplementary Figure S6A). Notably, the βArg244 flips ∼180° towards the editing site (Figure 3D).

The changes in residues located in the PheRS editing domain alter how these residues interact with Tyr and the tRNA backbone of C75. βGlu334 plays an important role in tyrosine discrimination via the formation of hydrogen bonds with the hydroxyl group of Tyr as assessed by molecular docking studies (24). In our structure, βGlu334 shifts away from the editing site ∼5.3 Å (Figure 3D). The βHis265 stabilizes substrate binding through π-stacking interactions with the Tyr (Figure 3C) (23,24). Other well-conserved editing site residues form an antiparallel β-sheet that upon oxidation, appears to be disrupted (Figure 4A and B) (24). None of the editing site residues are oxidized but this global oxidation disrupts the hydrogen bonding network of the β-sheet, shifting the β-sheet away from the editing site by ∼4.5 Å (Figure 4C; Supplementary Figure S6B) (38). This movement creates a larger binding surface (increases from ∼204 Å^2 to ∼295 Å^2) (42) for the incorrect amino acid to be edited (Figure 4D and E). Despite the relatively moderate changes in the locations of the oxidized residues (Figure 2; Supplementary Figure S4), there is extensive rearrangement of β-

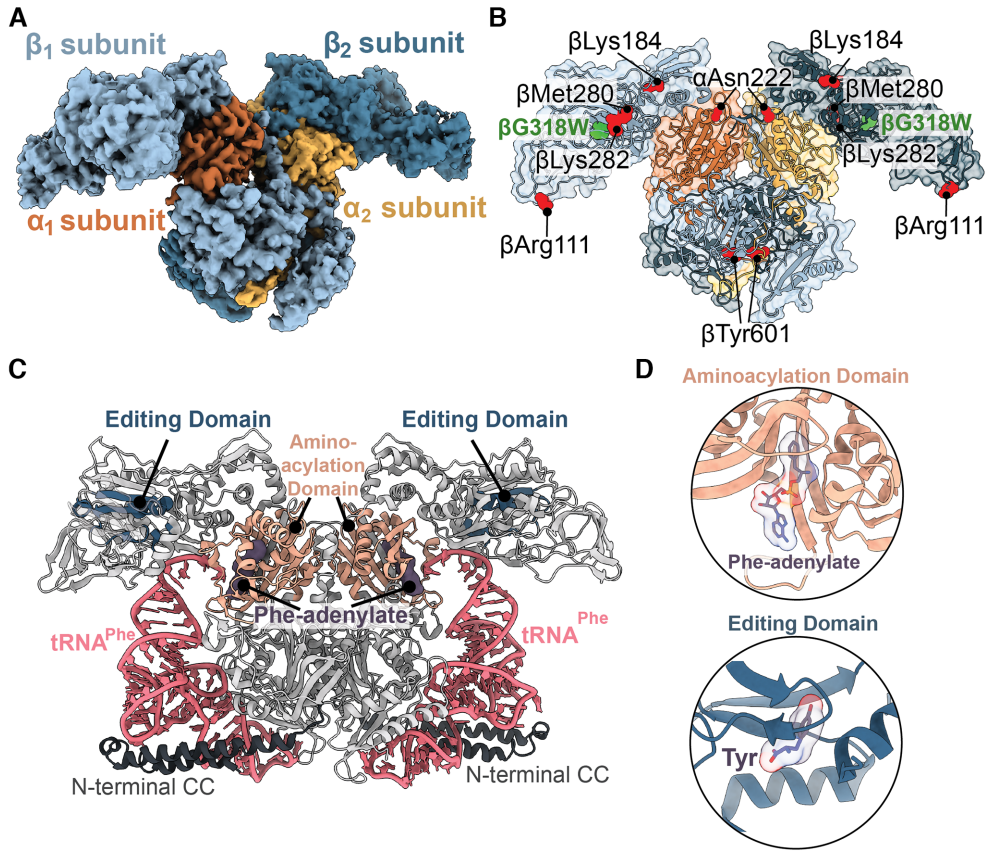

Figure 1. Overview of the PheRS βG318W structure. (**A**) The 3.6 Å map of the oxidized *S.* Typhimurium editing-deficient PheRS βG318W tetramer. PheRS is composed of two α-subunits (orange and yellow) and two β-subunits (light blue and dark blue). (**B**) Oxidized PheRS βG318W (green) with oxidized residues, as determined previously (25), shown as red spheres. (**C**) *T. thermophilus* PheRS (grey) containing Phe-adenylate (purple, surface) and $tRNA^{Phe}$ (pink) (PDB code 2IY5). The N-terminal coiled-coil extensions (N-terminal CC (dark grey); residues 1–88) in the α-subunits are resolved when bound to tRNA. (**D**) Aminoacylation (peach) and editing domains (dark blue) are shown with respective ligands, Phe-adenylate and Tyr, bound (purple, PDB code 2AMC).

subunit residues involved with editing activity that result in a larger editing domain.

PheRS oxidation induces structural changes in the α-subunit active site

The catalytic domain of the PheRS α-subunits form interactions with Phe and AMP, allowing for the specific addition of a phenylalanyl-adenylate to $tRNA^{Phe}$ (Figure 5A and B; Supplementary Figure S7A). The active site is composed of three regions: the motif 2 loop (residues 194–205), the second helical loop (h2, residues 145–158), and the phenylalanine-proline-phenylalanine (FPF) loop (residues 246–254) (Figure 5B–E; Supplementary Figure S7) (14,44,45). The only α-subunit residue that is oxidized is αAsn222, which is located outside the active site but its backbone conformation is not affected by oxidation (25) (Supplementary Figure S2B). However, global oxidation results in conformational differences within the phenylalanyl-adenylate binding pocket (Figure 5C–E).

In the motif 2 loop, αHis202, which normally forms hydrogen bonds with AMP, moves ∼2.1 Å away from the Phe-adenylate (Figure 5C; Supplementary Figure S7B). However, not all catalytic residues in the motif 2 loop are affected. For example, αPhe206, which forms π-stacking interactions with the adenosine, adopts the same conformation as non-oxidized PheRS (Figure 5C). The h2 and FPF loop of the phenylalanyl-adenylate binding pocket also undergo conformational shifts (Figure 5). The second helical loop (h2), a segment that undergoes rearrangement upon Phe and AMP binding (14,45), undergoes conformational changes upon oxidization despite that none of the h2 residues are oxidized (Figure 5D; Supplementary Figure S7C). Both αHis148 and αHis149 shift away from the active site ∼3.7 and ∼3.8 Å, respectively (Figure 5D). Normally, $tRNA^{Phe}$, and specifically the last nucleotide A76, is recognized by contacts from the side chain of αAsp154 located within h2 (Figure 5D; Supplementary Figure S8). In oxidized PheRS βG318W, αAsp154 shifts ∼4.5 Å away from the tRNA binding site. The FPF loop, which is conserved across all bacterial species (14), forms π-stacking interactions with Phe (Supplementary Figure S8). Within the FPF loop, αPhe248 shifts ∼2.7 Å away from where Phe binds, which would prevent this interaction (Figure 5E; Supplementary Figure S7D). These movements in the motif 2, h2 and FPF loops enlarge the phenylalanyl-adenylate binding pocket from ∼1560 to ∼1980 $Å^2$ (Figure 5F and G).

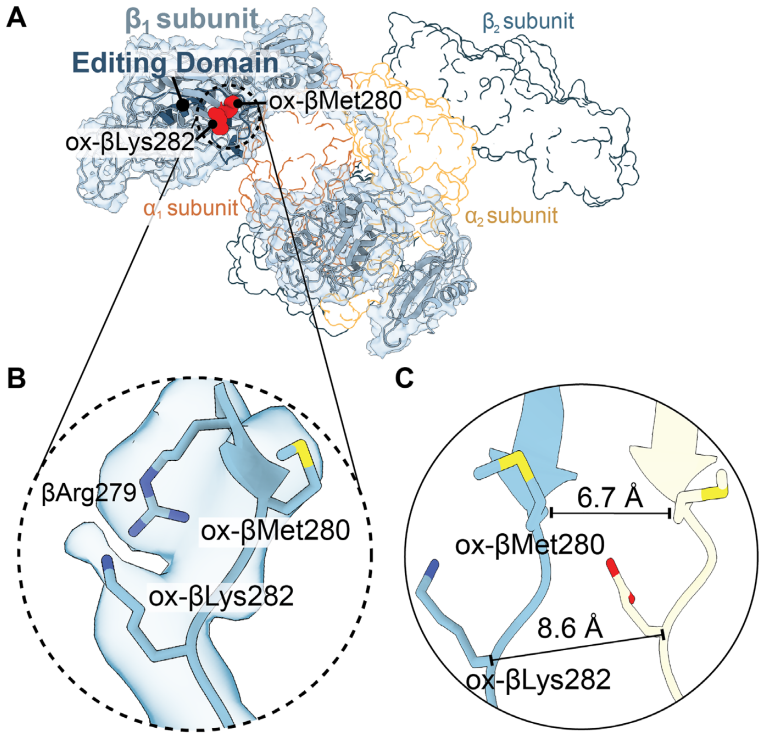

Figure 2. PheRS βMet280 and βLys282 residues located outside the editing domain move substantially upon oxidation. (**A**) Overview of the β_1 subunit map and model (light blue) with the editing domain (dark blue) and oxidized residues (red spheres). The other PheRS subunits are shown as outlines. (**B**) Map and model of ox-βMet280 and ox-βLys282 located in the editing domain. (**C**) Comparison of ox-βMet280 and ox-βLys282 (corresponding residue in *P. aeruginosa* is Glu281) with *P. aeruginosa* apo-PheRS (yellow, PDB code 4P73) revealing significant movements of ∼6.7 and ∼8.6 Å, respectively.

Upon oxidation, there is a 30% decrease in misacylation of $tRNA^{Phe}$ with Tyr (25). Discrimination between Phe and Tyr is facilitated by αGlu210 within h2 which hydrogen bonds to the bound amino acid to facilitate ligation (Figure5B and D; Supplementary Figure S8). In our structure, the position of αGlu210 moves to a position that would directly overlap with the hydroxyl group of Tyr (14) (Supplementary Figure S9) as compared to a *Escherichia coli* PheRS structure containing Phe and AMP (PBD code 3PCO). This new αGlu210 position may explain why misacylation decreases upon PheRS oxidation.

Similarities between oxidized S. Typhimurium PheRS and the *E. coli* PheRS–Phe–AMP complex

Oxidation causes both larger editing and aminoacylation sites as compared to apo-*Pa*PheRS as previously described (an increase of 204–295 $Å^2$ (Figure 4D and E) and an increase of 1560–1900 $Å^2$ (Figure 5F and G), respectively). Although all comparisons to this point have been of oxidized apo-PheRS βG318W to apo-*Pa*PheRS, interestingly, specific regions of oxidized apo-PheRS are slightly more similar to the structure of *Ec*PheRS complexed with ligands Phe and AMP (PDB code 3PCO (14), RMSD of ∼1.7 Å). While binding of Phe and AMP to *Ec*PheRS increases the editing (∼272 $Å^2$) and Phe-adenylate binding pocket (∼1700 $Å^2$), these sites are still smaller than when PheRS is oxidized (Supplementary Figures S10D and S11B).

One of the most striking changes between oxidized apo-PheRS and *Ec*PheRS bound to Phe and AMP is the placement of βMet280 and βLys282, residues that both become oxidized but are located outside the two catalytic sites (Figure 2). Normally the backbone of these residues dramatically changes upon binding of Phe and AMP (changes of 9.4 Å (βMet280) and 10.3 Å (βLys282)). Oxidation of βMet280 and βLys282 also influences their positions however, now these residues adopt similar positions as when Phe and AMP bind (Supplementary Figure S10A) (14). This movement places these residues closer towards the editing domains where tRNA binds despite not containing any ligands.

Comparison of Phe-AMP bound *Ec*PheRS with oxidized apo-PheRS also reveals changes of editing site residues that appear to enlarge the binding pocket and change how oxidized PheRS would engage either the amino acid or AMP (Supplementary Figure S10). First, the side chain of βHis265 flips away from the amino acid binding site (Supplementary Figure S10B), likely influencing recognition of the incorrect Tyr. This flipping may occur as PheRS transitions to prepare for hydrolysis of incorrectly bound Tyr. The βArg244 sidechain, which normally recognizes the tRNA backbone of nucleotide C75, is rotated ∼180° away in the absence of tRNA (Figure 3C). Oxidation of PheRS causes βArg244 to more resemble *Ec*PheRS-Phe-AMP despite lacking the tRNA (Supplementary Figure S10B). Lastly, oxidation cause the entire β-sheet comprising the editing domain to shift by ∼2.7–3.7 Å and rotate ∼45° thus placing it further away from the aminoacylated-tRNA binding site (Supplementary Figure S10C). Collectively, these changes create a larger editing site but with ac-

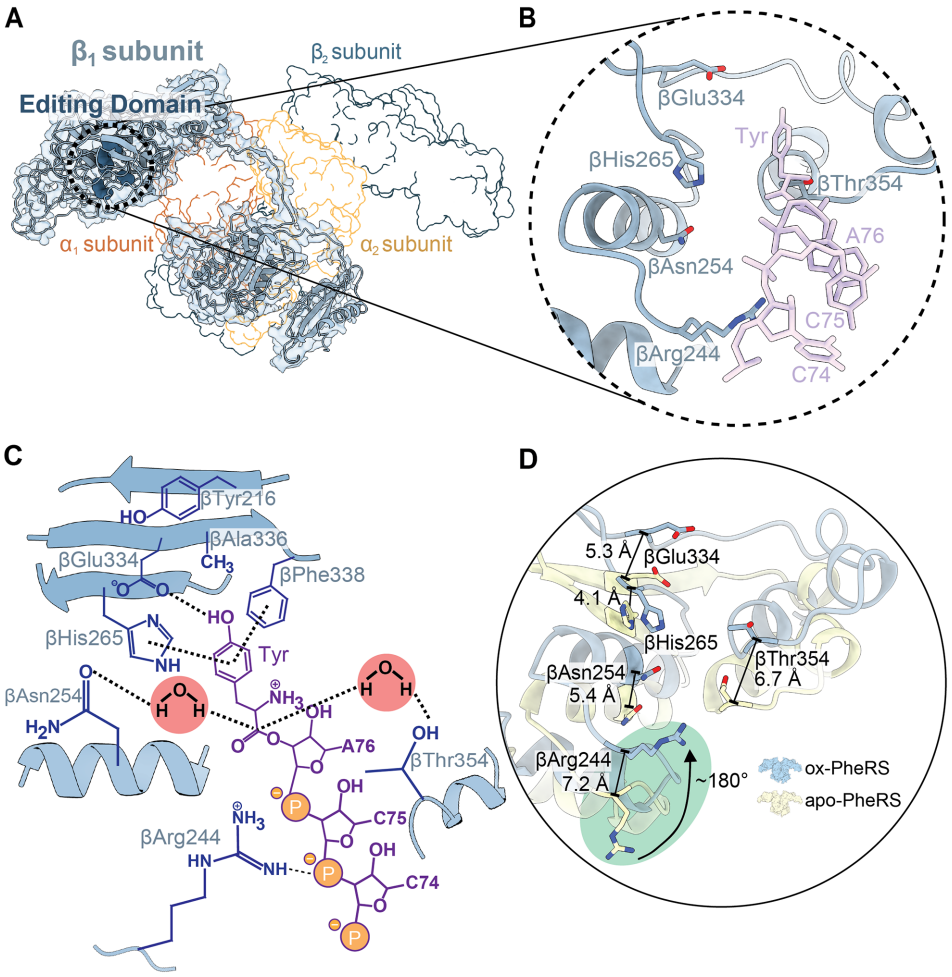

Figure 3. Localized active site conformational changes of the PheRS editing domain. (**A**) Oxidized *S.* Typhimurium editing-deficient PheRS βG318W β_1-subunit with corresponding map (light blue) and active site residues in the editing domain shown as spheres (dark blue). The other PheRS subunits are shown in outline. (**B**) Closeup of editing site residues with Tyr-tRNA^{Phe} docked into the editing site (PDB code 3HFZ, purple). (**C**) Overview of the editing site residues (blue) and interactions with a Tyr-tRNA^{Phe} CCA end (purple), and the two catalytic waters that carry out the reaction. (**D**) Residues of the editing domain of the oxidized *S.* Typhimurium PheRS compared to the *P. aeruginosa* apo-PheRS (yellow, PDB code 4P73) undergo a significant shift, particularly βArg244 which is shifted ∼7.2 Å and flipped ∼180° inwards towards the editing site (green circle).

tive site residues positioned in conformations to allow for the increase in editing activity of the oxidized PheRS.

DISCUSSION

To prevent protein mistranslation, aminoacyl-tRNA synthetases pair correct amino acids to their cognate tRNAs with high fidelity to ensure the correct addition of amino acids into proteins. Environmental stress, including oxidative stress, alters cellular amino acid pools and this change can affect the fidelity of gene expression. During oxidative stress, oxidation of Phe converts it to Tyr, increasing Tyr isomer levels and leads to an overall increase in tRNA^{Phe} misacylation (29). However, oxidation of PheRS compensates by increasing proofreading to reduce misacylated Tyr-tRNA^{Phe} from participating in protein synthesis. Several PheRS residues are oxidized and these modifications are found throughout PheRS and not localized solely at the active site (29). Since oxidation causes a hyperaccurate phenotype but there is no oxidation at the active sites, this suggests that allosteric changes may contribute to PheRS acquiring hyperaccuracy consistent with previous results that demonstrated global changes (25). Based upon these results, we set out to determine the cryo-EM structure of oxidized PheRS. Overall, we find that oxidation results in structural changes mainly in the β-subunit editing domain and to a lesser extent, the α-subunit aminoacylation active site. The β-subunit editing domain is enlarged where mischarged Tyr-tRNA^{Phe} would bind and its surface area increases by 50%. Oxidization also enlarges the phenylalanyl-adenylate binding pocket in the α-subunit by 30%. These enlargements are predicted to contribute to faster and efficient binding, while additional conformational changes of catalytic residues suggest an improvement in Tyr hydrolysis required to ligate the correct Phe. These results shed light on how *S.* Typhimurium is able to survive and grow in adverse environments.

Based on high structural homology between bacterial PheRS (49,50), it is likely that most bacterial PheRS enzymes have a similar hyperaccuracy phenotype under ox-

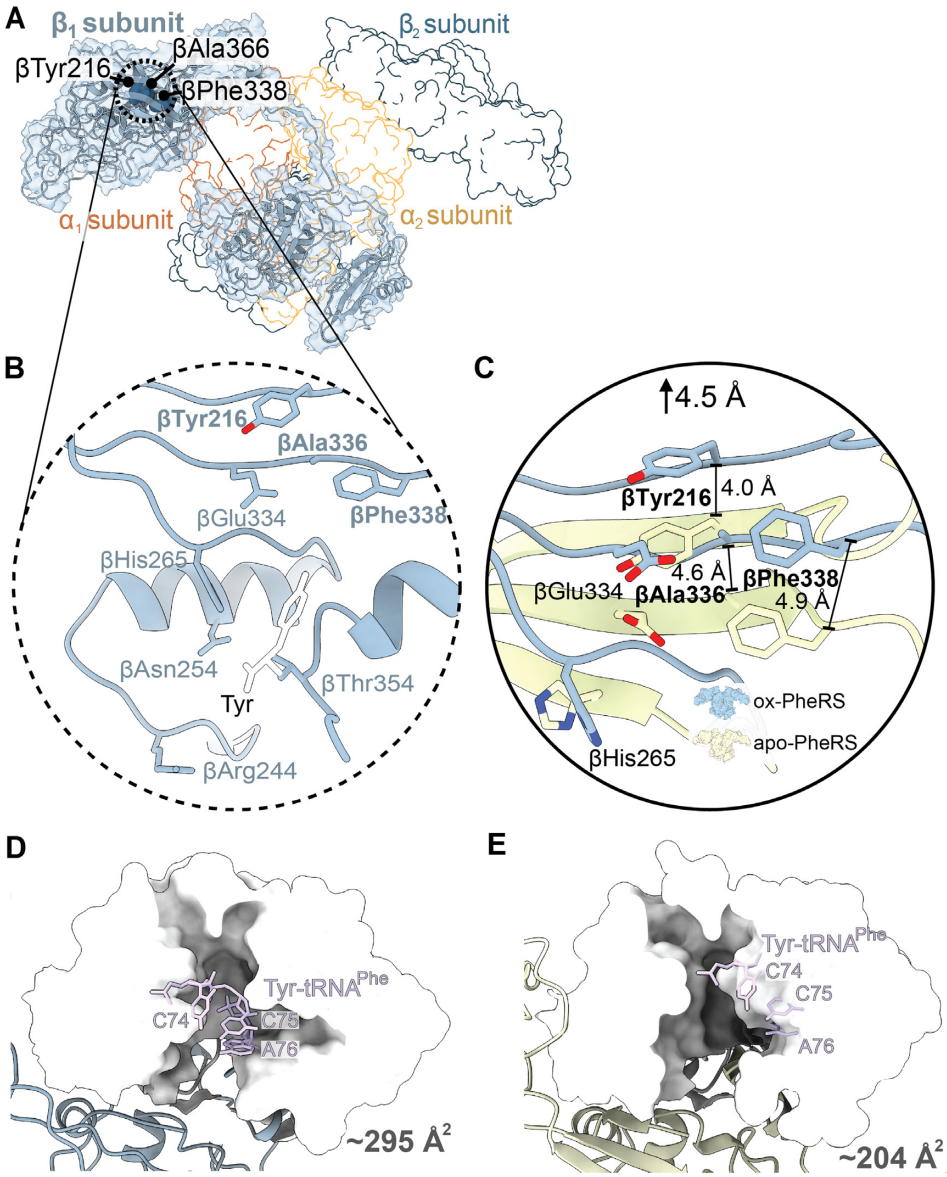

Figure 4. Oxidization of PheRS βG318W opens the editing domain leading to hyperaccuracy. (**A**) Structure of oxidized *S.* Typhimurium PheRS βG318W β_1-subunit with corresponding map density (blue) and catalytic residues that are implicated in editing activity shown as dark blue spheres, with other subunits shown in outline. (**B**) Closeup of the catalytic region with Tyr overlaid from a *T. thermophilus* PheRS-Tyr structure (white, PDB code 3HFZ). (**C**) The catalytic residues βTyr216, βAla336, and βPhe388 of the oxidized *S.* Typhimurium PheRS undergo a shift averaging ∼4.5 Å away from the editing domain compared to the *P. aeruginosa* apo-PheRS (PDB code 4P73, yellow). (**D**) Editing domain of oxidized PheRS βG318W shown as surface (white) with Tyr-tRNA^{Phe} docked in site (PDB code 3HFZ, purple). (**E**) Editing site residues of apo-PheRS shown as surface (white) with Tyr-tRNA^{Phe} docked into the editing site (PDB code 3HFZ, purple).

idative stress. Although there is typically high homology among mitochondrial and bacterial synthetases (51), PheRS is an exception as the mitochondrial and bacterial synthetase are divergent (52). Mitochondrial PheRS is a monomer and lacks an editing domain found in the tetrameric bacterial PheRS (52), and as a consequence, is unable to proofread misacylated tRNA^{Phe} (52). Although mitochondrial PheRS is oxidized during oxidative stress, this does not result in hyperaccuracy and oxidation can be reversed (25), restoring normal function.

While oxidation of other synthetases including ThrRS and AlaRS can occur, this does not result in hyperaccuracy, in contrast to PheRS. ThrRS is known to misacylate tRNA^{Thr} with Ser and contains a catalytic cysteine in the editing domain (53). Under oxidative conditions, this reactive cysteine is oxidized and thus prevents ThrRS editing ability (54), the opposite phenotype to what is observed with PheRS (25,53). AlaRS also relies on a critical cysteine residue to carry out editing activity upon misacylation of a Ser- or Gly-tRNA^{Ala} (55), but changes in AlaRS editing activity upon oxidation have not yet been reported. Changes in AlaRS editing activity are significantly more determinantal for bacteria viability compared to ThrRS (56). From a fitness perspective, maintenance of AlaRS editing activity is more important for bacterial survival, suggesting possible divergence in editing response under oxidation as com-

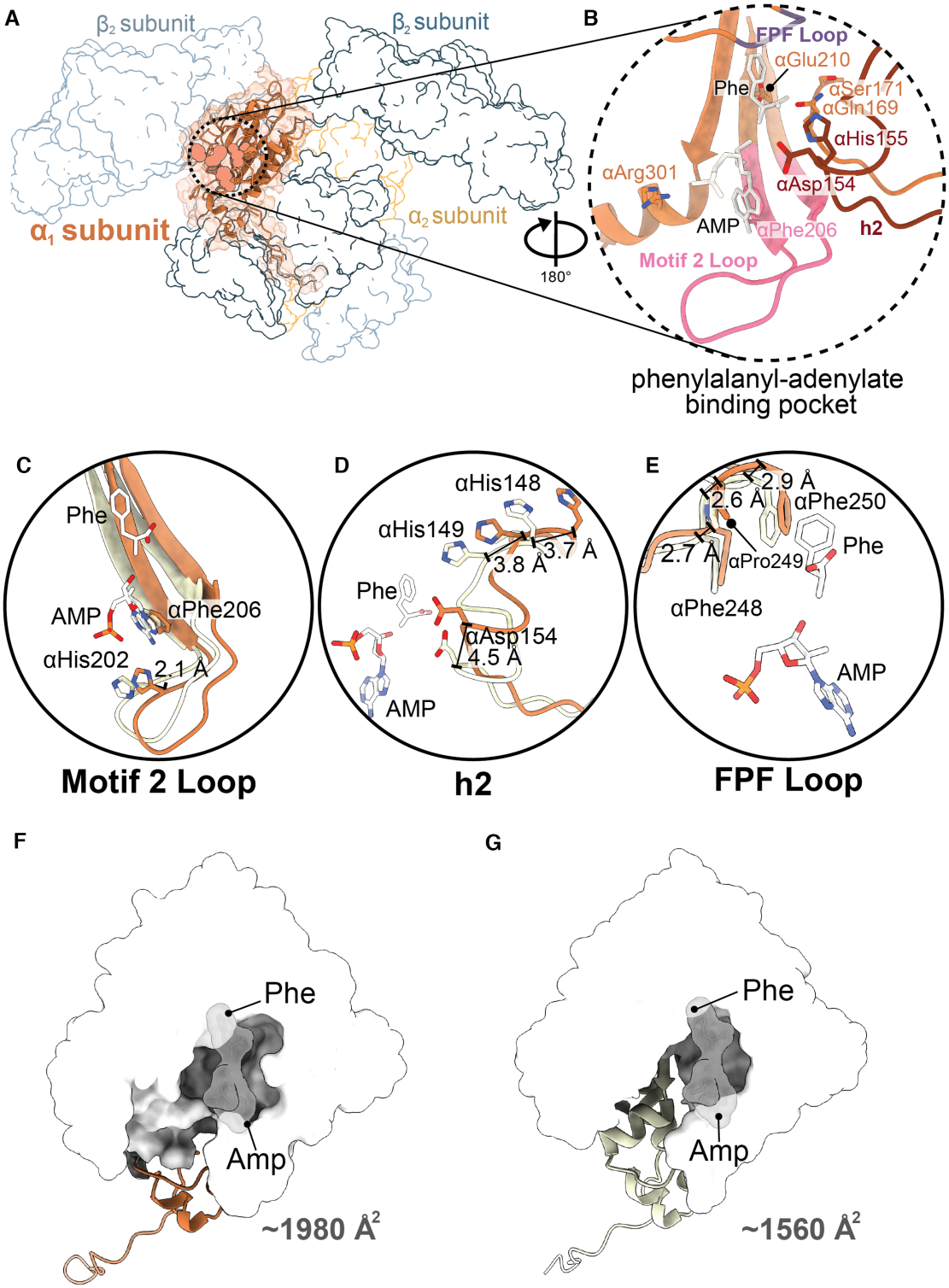

Figure 5. Conformational changes of the aminoacylation domain. (**A**) Structure of oxidized *S.* Typhimurium PheRS βG318W α_1-subunit and map (orange). Aminoacylation active site residues shown as spheres, with other subunits shown in outline. (**B**) Active site residues in the phenylalanyl-adenylate binding pocket (orange) with modeled AMP and Phe (PDB code 3PCO, white). The motif 2 loop (pink), helix 2 loop (h2, dark red), and FPF loop (purple) are shown. (**C**) The motif 2 loop shifts outwards by ∼2.1 Å from *P. aeruginosa* apo-PheRS (PDB code 4P73, yellow). (**D**) The h2 of oxidized PheRS has conformational rearrangements, 3.7 Å and 3.8 Å at αHis148 and αHis149, respectively, and 4.5 Å at αAsp154, away from the phenylalanyl-adenylate binding pocket compared to apo-PheRS (PDB code 4P73, yellow). (**E**) The FPF loop contains minor conformational changes, with 2.7, 2.6 and 2.9 Å shifts of the αPhe248, αPro249 and αPhe250, respectively, away from the phenylalanyl-adenylate binding pocket compared to apo-PheRS (PDB code 4P73, yellow) (**F**) Enlargement of the aminoacylation domain shown with surface (white) of oxidized PheRS βG318W, with AMP and Phe groups docked in and shown with surfaces (PDB code 3PCO, grey). (**G**) Enlargement of the aminoacylation domain shown as surface (white) of the apo-*Pa*PheRS (PDB code 4P73, yellow), with AMP and Phe groups docked in shown as surfaces (PDB code 3PCO, grey).

pared to ThrRS. Under normal growth conditions, PheRS editing activity is not vital for bacterial viability, but becomes required for growth under oxidative conditions (29). Translation accuracy under oxidative stress is vital for cellular survival, but among the class II aaRSs, only PheRS undergoes a gain of function change. The benefit of PheRS hyperaccuracy under conditions that directly increase the likelihood of mistranslation serves as a direct compensatory mechanism to decrease the likelihood of Tyr misincorporation; while ThrRS and possibly AlaRS are susceptible to oxidative stress, the Ser or Gly amino acid pools are not expected to change significantly, placing less selective pressure on these synthetases to compensate for misacylation under oxidative conditions.

Oxidation is a well characterized signal for proteins directly involved in the oxidative stress response including redox-operated switches that activate transcription of oxidative response elements (57). However, these mechanisms are indirect and contribute to a regulatory pathway that allows for increased cell survival under adverse conditions. PheRS represents one of the few examples of a functional protein that self-regulates as a feedforward mechanism to directly compensate against an adverse condition.

Responses to stress are typically analyzed at the level of gene expression (58,59). With oxidative stress, several genes including *oxyR*, *oxyS*, or *perR*, are directly regulated by oxidation of several cysteine residues allowing for transcription factor binding to promote the expression of proteins involved in metabolism or clearance of oxidative stress (60). The hyperaccuracy phenotype of PheRS under oxidative stress illustrates how important pathways in protein synthesis work to maintain proper gene expression. This ensures successful expression of oxidative response genes, which relies on accurate amino acid additions to growing nascent chain on the ribosome. Oxidized PheRS hyperaccuracy ensures that correct gene expression is not compromised by elevated and potentially toxic Tyr isomer misincorporation under oxidative stress. Hyperaccurate aminoacylation thus helps to increase survival, particularly for organisms regularly present in oxidative environments like *S.* Typhimurium, which can thrive in environments like a macrophage despite a host reactive oxygen species attack. Overall, the proper activation of stress responses, including increased proofreading activity of PheRS, increases *S.* Typhimurium survival and contributes to the overall fitness of the bacterium.

DATA AVAILABILITY

Atomic coordinates and maps for the reported cryo-EM structures have been deposited with the Protein Data bank under accession number 7N8Y and Electron Microscopy Data bank under accession number EMD-24249.

SUPPLEMENTARY DATA

Supplementary Data are available at NAR Online.

ACKNOWLEDGEMENTS

We thank Dunham lab member Dr Alexandra Kuzmishin Nagy for critical reading of the manuscript and Ha An Nguyen for technical support.

FUNDING

National Institutes of Health [R01GM065183 to M.I. and C.M.D., R01 GM093278 to C.M.D., 5T32 GM008602 to P.S., T32 AI106699 to P.S.]; Burroughs Wellcome Fund Investigator in the Pathogenesis of Infectious Disease award (to C.M.D.); Robert P. Apkarian Integrated Electron Microscopy Core (IEMC) at Emory University, which is subsidized by the School of Medicine and Emory College of Arts and Sciences. Funding for open access charge: National Institutes of Health.
Conflict of interest statement. None declared.

REFERENCES

1. McClain,W.H. (1993) Rules that govern tRNA identity in protein synthesis. *J. Mol. Biol.*, **234**, 257–280.
2. Cochella,L. and Green,R. (2005) Fidelity in protein synthesis. *Curr. Biol.*, **15**, R536–R540.
3. Jakubowski,H. and Goldman,E. (1992) Editing of errors in selection of amino acids for protein synthesis. *Microbiol. Rev.*, **56**, 412–429.
4. Schimmel,P.R. and Söll,D. (1979) Aminoacyl-tRNA synthetases: general features and recognition of transfer RNAs. *Annu. Rev. Biochem.*, **48**, 601–648.
5. Delarue,M. (1995) Aminoacyl-tRNA synthetases. *Curr. Opin. Struct. Biol.*, **5**, 48–55.
6. Ahel,I., Korencic,D., Ibba,M. and Söll,D. (2003) Trans-editing of mischarged tRNAs. *Proc. Natl. Acad. Sci. U.S.A.*, **100**, 15422–15427.
7. Eriani,G., Delarue,M., Poch,O., Gangloff,J. and Moras,D. (1990) Partition of tRNA synthetases into two classes based on mutually exclusive sets of sequence motifs. *Nature*, **347**, 203–206.
8. Fraser,T.H. and Rich,A. (1975) Amino acids are not all initially attached to the same position on transfer RNA molecules. *Proc. Natl. Acad. Sci. U.S.A.*, **72**, 3044–3048.
9. Sprinzl,M. and Cramer,F. (1975) Site of aminoacylation of tRNAs from Escherichia coli with respect to the 2′- or 3′-hydroxyl group of the terminal adenosine. *Proc. Natl. Acad. Sci. U.S.A.*, **72**, 3049–3053.
10. Bullwinkle,T.J. and Ibba,M. (2014) Emergence and evolution. *Top. Curr. Chem.*, **344**, 43–87.
11. Kaiser,F., Krautwurst,S., Salentin,S., Haupt,V.J., Leberecht,C., Bittrich,S., Labudde,D. and Schroeder,M. (2020) The structural basis of the genetic code: amino acid recognition by aminoacyl-tRNA synthetases. *Sci. Rep.*, **10**, 12647.
12. Fukai,S., Nureki,O., Sekine,S.-i., Shimada,A., Tao,J., Vassylyev,D.G. and Yokoyama,S. (2000) Structural basis for double-sieve discrimination of L-valine from L-isoleucine and L-threonine by the complex of tRNAVal and valyl-tRNA synthetase. *Cell*, **103**, 793–803.
13. Lincecum,T.L., Tukalo,M., Yaremchuk,A., Mursinna,R.S., Williams,A.M., Sproat,B.S., Van Den Eynde,W., Link,A., Van Calenbergh,S., Grøtli,M. *et al.* (2003) Structural and mechanistic basis of pre- and posttransfer editing by leucyl-tRNA synthetase. *Mol. Cell*, **11**, 951–963.
14. Mermershtain,I., Finarov,I., Klipcan,L., Kessler,N., Rozenberg,H. and Safro,M.G. (2011) Idiosyncrasy and identity in the prokaryotic phe-system: crystal structure of E. coli phenylalanyl-tRNA synthetase complexed with phenylalanine and AMP. *Protein Sci.*, **20**, 160–167.
15. Silvian,L.F., Wang,J. and Steitz,T.A. (1999) Insights into editing from an Ile-tRNA synthetase structure with tRNAIle and mupirocin. *Science*, **285**, 1074–1077.
16. Martinis,S.A. and Boniecki,M.T. (2010) The balance between pre- and post-transfer editing in tRNA synthetases. *FEBS Lett.*, **584**, 455–459.
17. Dock-Bregeon,A.-C., Sankaranarayanan,R., Romby,P., Caillet,J., Springer,M., Rees,B., Francklyn,C.S., Ehresmann,C. and Moras,D. (2000) Transfer RNA-mediated editing in threonyl-tRNA synthetase. The class II solution to the double discrimination problem. *Cell*, **103**, 877–884.
18. Beebe,K., Merriman,E., de Pouplana,L.R. and Schimmel,P. (2004) A domain for editing by an archaebacterial tRNA synthetase. *Proc. Natl. Acad. Sci. U.S.A.*, **101**, 5958–5963.
19. Beuning,P.J. and Musier-Forsyth,K. (2000) Hydrolytic editing by a class II aminoacyl-tRNA synthetase. *Proc. Natl. Acad. Sci. U.S.A.*, **97**, 8916–8920.

20. Smith,T.F. and Hartman,H. (2015) The evolution of Class II aminoacyl-tRNA synthetases and the first code. *FEBS Lett.*, **589**, 3499–3507.
21. Moor,N., Klipcan,L. and Safro,Mark G. (2011) Bacterial and eukaryotic phenylalanyl-tRNA synthetases catalyze misaminoacylation of tRNAPhe with 3,4-dihydroxy-L-phenylalanine. *Chem. Biol.*, **18**, 1221–1229.
22. Roy,H., Ling,J., Irnov,M. and Ibba,M. (2004) Post-transfer editing in vitro and in vivo by the β subunit of phenylalanyl-tRNA synthetase. *EMBO J.*, **23**, 4639–4648.
23. Kotik-Kogan,O., Moor,N., Tworowski,D. and Safro,M. (2005) Structural basis for discrimination of L-phenylalanine from L-tyrosine by phenylalanyl-tRNA synthetase. *Structure*, **13**, 1799–1807.
24. Ling,J., Roy,H. and Ibba,M. (2007) Mechanism of tRNA-dependent editing in translational quality control. *Proc. Natl. Acad. Sci. U.S.A.*, **104**, 72–77.
25. Steiner,R.E., Kyle,A.M. and Ibba,M. (2019) Oxidation of phenylalanyl-tRNA synthetase positively regulates translational quality control. *Proc. Natl. Acad. Sci. U.S.A.*, **116**, 10058–10063.
26. Slauch,J.M. (2011) How does the oxidative burst of macrophages kill bacteria? Still an open question. *Mol. Microbiol.*, **80**, 580–583.
27. Winter,S.E., Thiennimitr,P., Winter,M.G., Butler,B.P., Huseby,D.L., Crawford,R.W., Russell,J.M., Bevins,C.L., Adams,L.G., Tsolis,R.M. *et al.* (2010) Gut inflammation provides a respiratory electron acceptor for Salmonella. *Nature*, **467**, 426–429.
28. Ling,J. and Söll,D. (2010) Severe oxidative stress induces protein mistranslation through impairment of an aminoacyl-tRNA synthetase editing site. *Proc. Natl. Acad. Sci. U.S.A.*, **107**, 4028–4033.
29. Bullwinkle,T.J., Reynolds,N.M., Raina,M., Moghal,A., Matsa,E., Rajkovic,A., Kayadibi,H., Fazlollahi,F., Ryan,C., Howitz,N. *et al.* (2014) Oxidation of cellular amino acid pools leads to cytotoxic mistranslation of the genetic code. *eLife*, **3**, e02501.
30. Ghosh,R. and Mitchell,D.L. (1999) Effect of oxidative DNA damage in promoter elements on transcription factor binding. *Nucleic Acids Res.*, **27**, 3213–3218.
31. Nawrot,B., Sochacka,E. and Düchler,M. (2011) tRNA structural and functional changes induced by oxidative stress. *Cell. Mol. Life Sci.*, **68**, 4023–4032.
32. Tanaka,M., Chock,P.B. and Stadtman,E.R. (2007) Oxidized messenger RNA induces translation errors. *Proc. Natl. Acad. Sci. U.S.A.*, **104**, 66–71.
33. Vogel,C., Silva,G.M. and Marcotte,E.M. (2011) Protein expression regulation under oxidative stress. *Mol. Cell. Proteomics*, **10**, M111.009217.
34. Steele-Mortimer,O. (2008) The Salmonella-containing vacuole: moving with the times. *Curr. Opin. Microbiol.*, **11**, 38–45.
35. Scheres,S.H.W. (2012) RELION: implementation of a Bayesian approach to cryo-EM structure determination. *J. Struct. Biol.*, **180**, 519–530.
36. Li,X., Mooney,P., Zheng,S., Booth,C.R., Braunfeld,M.B., Gubbens,S., Agard,D.A. and Cheng,Y. (2013) Electron counting and beam-induced motion correction enable near-atomic-resolution single-particle cryo-EM. *Nat. Methods*, **10**, 584–590.
37. Zhang,K. (2016) Gctf: real-time CTF determination and correction. *J. Struct. Biol.*, **193**, 1–12.
38. Abibi,A., Ferguson,A.D., Fleming,P.R., Gao,N., Hajec,L.I., Hu,J., Laganas,V.A., McKinney,D.C., McLeod,S.M., Prince,D.B. *et al.* (2014) The role of a novel auxiliary pocket in bacterial phenylalanyl-tRNA synthetase druggability. *J. Biol. Chem.*, **289**, 21651–21662.
39. Pettersen,E.F., Goddard,T.D., Huang,C.C., Couch,G.S., Greenblatt,D.M., Meng,E.C. and Ferrin,T.E. (2004) UCSF Chimera—a visualization system for exploratory research and analysis. *J. Comput. Chem.*, **25**, 1605–1612.
40. Adams,P.D., Afonine,P.V., Bunkóczi,G., Chen,V.B., Echols,N., Headd,J.J., Hung,L.-W., Jain,S., Kapral,G.J., Grosse Kunstleve,R.W. *et al.* (2011) The Phenix software for automated determination of macromolecular structures. *Methods*, **55**, 94–106.
41. Emsley,P., Lohkamp,B., Scott,W.G. and Cowtan,K. (2010) Features and development of Coot. *Acta Crystallogr., Sect. D: Biol. Crystallogr.*, **66**, 486–501.
42. Goddard,T.D., Huang,C.C., Meng,E.C., Pettersen,E.F., Couch,G.S., Morris,J.H. and Ferrin,T.E. (2018) UCSF ChimeraX: meeting modern challenges in visualization and analysis. *Protein Sci.*, **27**, 14–25.
43. Meng,E.C., Pettersen,E.F., Couch,G.S., Huang,C.C. and Ferrin,T.E. (2006) Tools for integrated sequence-structure analysis with UCSF Chimera. *BMC Bioinf.*, **7**, 339.
44. Mosyak,L., Reshetnikova,L., Goldgur,Y., Delarue,M. and Safro,M.G. (1995) Structure of phenylalanyl-tRNA synthetase from *Thermus thermophilus*. *Nat. Struct. Biol.*, **2**, 537–547.
45. Goldgur,Y., Mosyak,L., Reshetnikova,L., Ankilova,V., Lavrik,O., Khodyreva,S. and Safro,M. (1997) The crystal structure of phenylalanyl-tRNA synthetase from Thermus thermophilus complexed with cognate tRNAPhe. *Structure*, **5**, 59–68.
46. Kreutzer,R., Kruft,V., Bobkova,E.V., Lavrik,O.I. and Sprinzl,M. (1992) Structure of the phenylalnyl-tRNA synthetase genes from *Thermus thermophilus* HB8 and their expression in Escherichia coli. *Nucleic Acids Res.*, **20**, 4173–4178.
47. Khodyreva,S.N., Moor,N.A., Ankilova,V.N. and Lavrik,O.I. (1985) Phenylalanyl-tRNA synthetase from E. coli MRE-600: analysis of the active site distribution on the enzyme subunits by affinity labelling. *Biochim. Biophys. Acta*, **830**, 206–212.
48. Moor,N., Kotik-Kogan,O., Tworowski,D., Sukhanova,M. and Safro,M. (2006) The crystal structure of the ternary complex of phenylalanyl-tRNA synthetase with tRNAPhe and a phenylalanyl-adenylate analogue reveals a conformational switch of the CCA end. *Biochemistry*, **45**, 10572–10583.
49. Klipcan,L., Moor,N., Kessler,N. and Safro,M.G. (2009) Eukaryotic cytosolic and mitochondrial phenylalanyl-tRNA synthetases catalyze the charging of tRNA with the meta-tyrosine. *Proc. Natl. Acad. Sci. U.S.A.*, **106**, 11045–11048.
50. Neubauer,C., Gao,Y.-G., Andersen,K.R., Dunham,C.M., Kelley,A.C., Hentschel,J., Gerdes,K., Ramakrishnan,V. and Brodersen,D.E. (2009) The structural basis for mRNA recognition and cleavage by the ribosome-dependent endonuclease RelE. *Cell*, **139**, 1084–1095.
51. Kartvelishvili,E., Peretz,M., Tworowski,D., Moor,N. and Safro,M. (2016) Chimeric human mitochondrial PheRS exhibits editing activity to discriminate nonprotein amino acids. *Protein Sci.*, **25**, 618–626.
52. Roy,H., Ling,J., Alfonzo,J. and Ibba,M. (2005) Loss of editing activity during the evolution of mitochondrial phenylalanyl-tRNA synthetase. *J. Biol. Chem.*, **280**, 38186–38192.
53. Wu,J., Fan,Y. and Ling,J. (2014) Mechanism of oxidant-induced mistranslation by threonyl-tRNA synthetase. *Nucleic Acids Res.*, **42**, 6523–6531.
54. Sankaranarayanan,R., Dock-Bregeon,A.C., Romby,P., Caillet,J., Springer,M., Rees,B., Ehresmann,C., Ehresmann,B. and Moras,D. (1999) The structure of threonyl-tRNA synthetase-tRNA(Thr) complex enlightens its repressor activity and reveals an essential zinc ion in the active site. *Cell*, **97**, 371–381.
55. Pasman,Z., Robey-Bond,S., Mirando,A.C., Smith,G.J., Lague,A. and Francklyn,C.S. (2011) Substrate specificity and catalysis by the editing active site of alanyl-RNA synthetase from *Escherichia coli*. *Biochemistry*, **50**, 1474–1482.
56. Kelly,P., Backes,N., Mohler,K., Buser,C., Kavoor,A., Rinehart,J., Phillips,G., Ibba,M. and Merrikh,H. (2019) Alanyl-tRNA synthetase quality control prevents global dysregulation of the *Escherichia coli* proteome. *mBio*, **10**, e02921–e02919.
57. Pomposiello,P.J. and Demple,B. (2001) Redox-operated genetic switches: the SoxR and OxyR transcription factors. *Trends Biotechnol.*, **19**, 109–114.
58. Murray,J.I., Whitfield,M.L., Trinklein,N.D., Myers,R.M., Brown,P.O. and Botstein,D. (2004) Diverse and specific gene expression responses to stresses in cultured human cells. *Mol. Biol. Cell*, **15**, 2361–2374.
59. Majmundar,A.J., Wong,W.J. and Simon,M.C. (2010) Hypoxia-inducible factors and the response to hypoxic stress. *Mol. Cell*, **40**, 294–309.
60. Mongkolsuk,S. and Helmann,J.D. (2002) Regulation of inducible peroxide stress responses. *Mol. Microbiol.*, **45**, 9–15.